MIJST
MIST International Journal of Science and Technology

A Preliminary Assessment of Power Savings by Flettner Rotors Installed on a Cargo Ship

Mahin Hasan Moon*, Sikder Ariyan Zaman, Md. Daluar Hussain, and Md. Mezbah Uddin

Department of Naval Architecture and Marine Engineering, Military Institute of Science and Technology (MIST), Dhaka-1216, Bangladesh

Corresponding Email: *mahinhasan201924006@gmail.com*

ARTICLE INFO

Article History:

Received: 21st January 2025
Revised: 29th May 2025
Accepted: 02nd June 2025
Published: 30th June 2025

Keywords:

Energy-efficient Shipping
Flettner Rotor
Emission Reduction
Fuel Savings
Rotor to Rotor Interactions

ABSTRACT

In response to increasingly stringent environmental regulations by the International Maritime Organization (IMO), this study presents a preliminary assessment of Flettner rotors as a viable wind-assisted propulsion system for cargo ships. Using RANS-based Computational Fluid Dynamics (CFD), the aerodynamic performance of various rotor configurations is evaluated under different wind speeds, spin ratios, and angles of attack. Initially, an isolated 2D and 3D rotor at model scale are simulated for various operating conditions. A grid convergence study is conducted as part of the CFD results verification process. A cargo ship fitted with Flettner rotors is simulated to compute resistance and to evaluate rotor to rotor interaction. The obtained results and analyses demonstrate that, under optimal conditions, Flettner rotors have the potential to reduce fuel consumption and emissions by around 20%, significantly enhancing propulsive efficiency.

1. INTRODUCTION

Emissions from international shipping increased from 977 million tons in 2012 to 1,076 million tons in 2018 (Joung et al., 2020). During the same period, the share of shipping emissions in global anthropogenic emissions grew from 2.76% to 2.89% (Joung et al., 2020; Hussain & Amin, 2021; Kolodziejski & Sosnowski, 2025). According to the Energy Efficiency Design Index (EEDI) requirements, newly built ships must be 20% more efficient by 2020 and 30% more efficient by 2025 in terms of CO_2 emissions and overall air pollution (Joung et al., 2020, Hussain & Amin, 2021). To meet these International Maritime Organization (IMO) mandates, various approaches have been explored to improve energy efficiency and reduce fuel consumption and emissions. Notable methods include hull form optimization, implementation of innovative energy-saving devices, application of advanced coatings and lubricants on hull surfaces, and the use of renewable energy sources (Hussain et al., 2022; Wang et al., 2024).

Among these, the utilization of wind energy has emerged as one of the most promising strategies for reducing fuel consumption and addressing environmental challenges (Bordogna et al., 2019). Of the available wind-assisted ship propulsion technologies, wing sails and Flettner rotors are considered the most practical and reliable. Several studies on wing sail-assisted ships report potential fuel savings ranging from 20% to 30%, depending on wind speed, direction, and route (Hussain & Amin, 2021). A total of 38 ships have been retrofitted with Flettner rotors between 2018 and 2025 (Kolodziejski & Sosnowski, 2025). It has been reported that fuel savings and emission reductions of up to 10–20% can be achieved under real sea conditions using Flettner rotors (Hussain et al., 2018; Kolodziejski & Sosnowski, 2025). Figure 1 shows a 130 m RoLo (Roll-on/Lift-off) vessel, the E-Ship, equipped with four 35 m rotors by a German company in 2010, achieving a total fuel saving of approximately 15% (Kolodziejski & Sosnowski, 2025).

Figure 1: The E-Ship 1
(Source: https://www.fotocommunity.de/photo/e-ship-1-manfred-blochwitz/35628151)

Two other cargo ships, known as M/V Epanastasea and M/V Alcyone, were fitted with two 30 m × 5 m rotors each, and both reported a reduction in fuel consumption of about 8–10% during real-world operations (Kolodziejski & Sosnowski, 2025). The proven performance of rotor-assisted ships in real-world operations has encouraged the maritime research community to rigorously investigate such technologies, with the aim of improving designs and optimizing rotor configurations to maximize fuel savings. An increasing number of conceptual studies, both experimental and numerical, are being conducted to enhance rotor design and overall performance (Hussain & Amin, 2021).

Bordogna et al. (2019) carried out wind tunnel experiments on a large-scale Flettner rotor (1 m diameter, 3.73 m span) to evaluate aerodynamic performance at Reynolds numbers up to 1.0×10^6, focusing on critical and supercritical regimes. The study found that lift coefficients were mostly unaffected by Reynolds number for velocity ratios $k > 2.5$, but drag coefficients showed significant sensitivity across the tested flow conditions. The power coefficient was found to scale with the cube of the tangential velocity and remained largely independent of Reynolds number or whether the rotor was spinning in still or moving air. Chen et al. (2023) conducted an experimental study to evaluate the aerodynamic performance of large-scale Flettner rotors for marine applications, focusing on single and dual rotor configurations under varying flow conditions. Using wind tunnel tests at Reynolds numbers ranging from 9.33×10^4 to 3.15×10^5, they investigated the effects of velocity ratio (k), aspect ratio (L/D), and endplate diameter ratio (D_e/D) on lift, and drag. The optimal aerodynamic performance occurred at $k = 1.5–2.0$, with the highest lift-to-drag ratio and resultant force angle around 70°. For dual rotor setups, interference effects were found to significantly alter the aerodynamic forces, particularly when the spacing ratio (S/D) was low and the wind incidence angle was aligned with the rotor axis. Their results suggest that well-configured Flettner rotors can generate substantial aerodynamic thrust suitable for ship propulsion, offering potential fuel savings of up to 20% under ideal conditions (Chen et al., 2023).

Several numerical studies have been conducted to evaluate the aerodynamic characteristics of Flettner rotors, their performance as auxiliary propulsion devices, and the interactions between multiple rotors installed on ships (Traut et al., 2014; De Marco et al., 2016; Copuroglu & Pesman, 2018; Lu & Ringsberg, 2019; Li et al., 2021;e Tillig & Ringsberg, 2020; Kume et al., 2022). A study on the prediction of a ship's roll motion and the performance of Flettner rotors was conducted by Copuroglu and Pesman (2018). The study investigated a sample rotor with a diameter of 4 m and a height of 27 m, equipped with a Thom disc. While the rotors had no significant non-linear effect on roll motion, the driving force performance of the Flettner rotors was found to decrease during rolling conditions (Copuroglu & Pesman, 2018). De Marco et al. (2016) performed a systematic numerical study to identify the most influential parameters affecting Flettner rotor performance and reported that an additional forward thrust of up to 30% of the ship's resistance can be achieved within the operational speed range on actual routes. However, their prediction of the drag coefficient (C_D) exhibited the highest numerical uncertainty, which was primarily attributed to mesh-related errors. Kume et al. (2022) conducted a combined experimental and RANS-based CFD investigation on a VLCC equipped with four rotors, demonstrating that aerodynamic forces generated by the rotors vary significantly with velocity ratio and apparent wind angle. Their study confirmed that CFD predictions at model-scale Reynolds numbers can reliably reproduce wind tunnel results, supporting their use for evaluating rotor-assisted ship performance even at low Reynolds numbers.

Based on the importance of selecting optimal rotor parameters and deck configurations, this paper aims to evaluate the performance of rotor-assisted ships using RANS-based CFD simulations with a commercial solver. A systematic approach is adopted: beginning with the simulation of a 2D cylindrical rotor, followed by 3D rotor modeling, and finally, integration of the rotors onto a cargo vessel known as Japan Bulk Carrier (JBC) in two different configurations. Numerical simulations are performed for the ship with and without rotors, under various spin ratios and wind speeds, to explore optimal conditions. A mesh convergence and basic verification study is also conducted to ensure computational consistency. The results suggest that rotor-assisted propulsion can potentially reduce fuel consumption by over 20%. While the findings are preliminary and the study has limitations in robustness and validation, the outcomes provide valuable insights and direction for future investigations aimed at practical implementation of wind-assisted propulsion systems.

2. PHYSICS OF ROTOR SAIL SYSTEM

Figure 2 illustrates the detailed physics of a Flettner rotor and a rotor-assisted ship. As shown in Figure 2(a), a Flettner rotor is a rotating cylinder that generates a lift force perpendicular to the apparent wind direction due to the Magnus effect. When wind flows over the rotating surface, circulation is induced around the cylinder, resulting in a lift force, F.

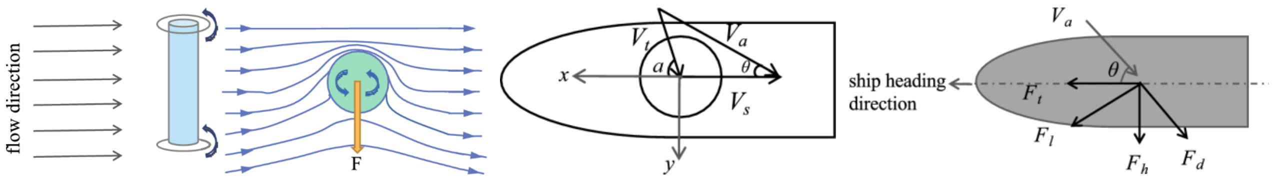

Figure 2: Physics of rotor assisted ship (a) Magnus effect mechanism of a rotor, (b) wind velocity triangle and (c) force components acting on the ship from rotor. (Adopted from Li et al., 2024)

Figure 2(b) shows the velocity triangle diagram for typical wind assisted ship, where V_s is the ship velocity, V_t is the true wind velocity, V_a is the apparent wind velocity and θ is the apparent wind angle (relative to ship heading).

Applying vector addition in Fig. 2(b):

$$\vec{V_a} = \vec{V_t} - \vec{V_s} \quad (1)$$

The magnitude of apparent wind can be written as (Seddiek & Ammar, 2021):

$$V_a = \sqrt{V_t^2 + V_s^2 - 2V_t V_s \cos\theta} \quad (2)$$

where, θ is the direction of apparent wind angle (from ship bow) and defined as:

$$\theta = \tan^{-1}\left(\frac{V_t \sin\theta}{V_t \cos\theta - V_s}\right) \quad (3)$$

Figure 2(c) shows force components from rotor, where F_t thrust (component in ship direction), F_l lift (due to Magnus effect), F_d rotor drag and F_h heeling force (lateral). Using simple trigonometry (Li et al., 2024):

$$F_t = F_l \cos\theta - F_d \sin\theta \quad (4)$$

$$F_h = F_l \sin\theta - F_d \sin\theta \quad (5)$$

Lift and drag are computed using the following expressions (Li et al., 2024):

$$F_l = \frac{1}{2}\rho\, A\, C_L V_a^2 \quad (6)$$

$$F_d = \frac{1}{2}\rho\, A\, C_D V_a^2 \quad (7)$$

where, ρ is the air density, A projected area of the rotor which is typically rotor diameter (D) × height (L), C_L lift coefficients and C_D drag coefficients. Lift coefficient depends strongly on spin ratio and defined as (Li et al., 2024):

$$\alpha = \frac{\omega R}{V_a} \quad (8)$$

where, ω angular velocity of the rotor and R is the rotor radius. Now to compute the net power savings from rotor, one must consider the power requires to rotate the rotor. The total power required to rotate a Flettner rotor is primarily used to overcome mechanical and aerodynamic torque. According to Lele & Rao (2017), the power required (P_{con}) to rotate a rotor is given as:

$$P_{con} = F_f U_{rot} \quad (9)$$

$$U_{rot} = \alpha V_a \quad (10)$$

$$F_f = \frac{c_f \rho_a U_{rot}^2}{2} A_r \quad (11)$$

$$c_f = \frac{0.455}{(\log(Re))^{2.58}} - \frac{1700}{Re} \quad (12)$$

$$Re = \frac{\rho_a \alpha V_a l}{\mu_a} \quad (13)$$

where, F_f is the rotor the frictional force, A_r rotor surface area, l is the rotor characteristic length, α is the spin ratio, and the subscript a with each term indicates air.

3. GOVERNING EQUATIONS OF NUMERICAL SIMULATIONS

In this study, Unsteady Reynolds-Averaged Navier Stokes (URANS) simulations are performed using SST k-ω tubulence model with an implicit unsteady formulation and second-order spatial and temporal discretization. The set of RANS equations for incompressible flow are given as (Hussain et al., 2022):

$$\frac{\partial \bar{u}_i}{\partial x_i} = 0 \quad (14)$$

$$\frac{\partial \bar{u}_i}{\partial t} + u_j \frac{\partial u_i}{\partial x_j} + \frac{1}{\rho}\frac{\partial p}{dx_i} = \frac{\partial}{dx_j}\left[(\nu + \nu_t)\left(\frac{\partial u_i}{\partial x_j} + \frac{\partial u_j}{\partial x_i}\right)\right] \quad (15)$$

where, $\bar{u}_i$ is the mean velocity components, ν is the molecular viscosity, ν_t is turbulent eddy viscosity, and p is the pressure. The SST (Shear Stress Transport) model blends the standard $k-\omega$ model for near wall region with $k-\epsilon$ model in the far field using a blending function. The turbulent kinetic energy equation (k) (Mentor, 1994):

$$\frac{\partial k}{\partial t} + u_j \frac{\partial k}{\partial x_j} = P_k \beta^* k\omega + \frac{\partial}{dx_j}\left[(\nu + \alpha_k \nu_t)\frac{\partial k}{\partial x_j}\right] \quad (16)$$

where, P_k production term of turbulence, $\alpha,\ \beta^*$ and α_k are model constant which are 0.52, 0.09 and 0.5 respectively. The equation of specific dissipation rate equation (ω) (Mentor, 1994):

$$\frac{\partial \omega}{\partial t} + u_j \frac{\partial \omega}{\partial x_j} = \alpha \frac{\omega}{k} P_k - \beta\omega^2 + \frac{\partial}{dx_j}\left[(\nu + \alpha_\omega \nu_t)\frac{\partial \omega}{\partial x_j}\right]$$
$$+2(1 - F_1)\frac{\sigma_\omega}{\omega}\frac{\partial k}{\partial x_j}\frac{\partial \omega}{\partial x_j} \quad (17)$$

where, F_1 is the blending function used to switch between $k-\omega$ model and $k-\epsilon$ model, β and σ_ω are model coefficients with a value of 0.072 and 0.5, respectively. A detailed and comprehensive description of the model can be found in Menter (1994).

4. WORK METHODOLOGY

Figure 3 summarizes the over workflow that is followed to perform this numerical study. The computational study begins with the selection of rotor parameters and operating conditions, including dimensions, spin ratios, and wind speeds relevant to performance evaluation. Next, 2D and 3D simulations of isolated rotors are performed to understand their aerodynamic behavior and generate force data. A suitable ship model (Japan Bulk Carrier (JBC)) and design parameters are then selected, followed by a resistance computation of the bare hull to establish a baseline. Subsequently, rotors are installed on the ship model, and the towing resistance of the rotor-assisted configuration is evaluated. Finally, a self-propulsion computation is conducted to quantify the net thrust contribution from the rotors and estimate potential fuel savings.

5. ROTOR DESIGN AND SHIP PARTICULARS

A rotor of 30 × 5 m rotor with an aspect ratio of 6 was chosen for this study and the design parameters are chosen based on some existing literature as reported in the review paper of Kolodziejski & Sosnowski (2025). Figure 4 shows the design of a rotor sail that was modeled and used in this study. The Japan Bulk Carrier (JBC) is used as reference ship (Hirata et al., 2020) and the main particulars with operating conditions are summarized in Table 1. All simulations were carried out at a model scale of 1:40 for the ship with rotor cases. A total of four rotors were installed on the deck in different configuration arrangements, as illustrated in Figure 5.

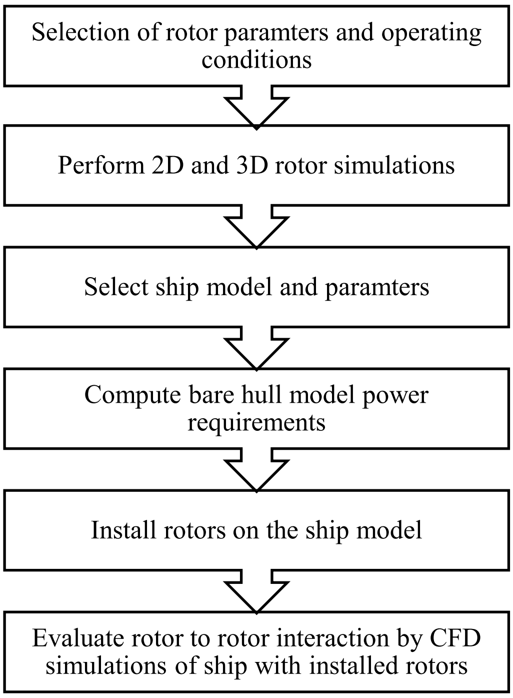

Figure 3: Overview of the workflow for the study

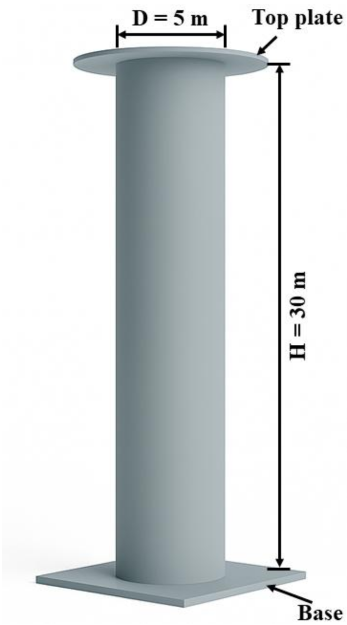

Figure 4: Designed rotor used in this study

Table 1: Ship Particulars (Hirata et al., 2020)

Particulars	Full-scale	Model Scale	Units
Length (Lpp)	280.0	7.00	m
Beam (B)	45.0	1.125	m
Draft (d)	16.5	0.412	m
Speed (V_s)	7.459	1.179	m/s

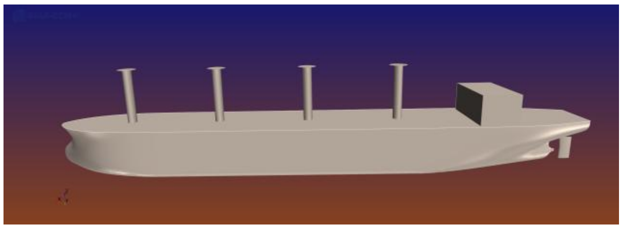

(a)

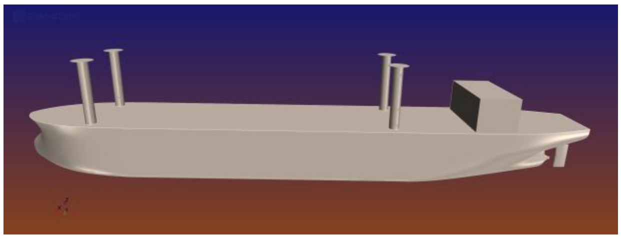

(b)

Figure 5: Two different rotor installation configurations on the deck: in-line arrangement (top) and 2 × 2 staggered arrangement (bottom)

6. RESULTS AND DISCUSSION

6.1 Rotor Performance Assessment

6.1.1 Computational setup and Mesh Description

In the preliminary assessment of rotor performance, both 2-D and 3-D simulations of a single rotor were performed under two different wind speeds: 1.26 m/s and 1.90 m/s in model scale, which corresponds 8 m/s and 12 m/s in full scale, respectively. The spin ratio varied from 1 to 5 to evaluate the aerodynamic performance and angles of attack were 120, 135, 150, 165 and 180 degrees. Figure 5 shows the computational set up configuration and domain used for the simulation of a single 2-D rotor. The domain is rectangular, with the rotor positioned approximately 4.5×D (rotor diameter) downstream from the velocity inlet, where D is the rotor diameter. The outlet boundary is located 27×D downstream of the rotor to allow for fully developed wake flow. The domain extends to 7×D in both vertical directions to minimize blockage effects. Symmetry boundary conditions are applied at the top and bottom, while a no-slip boundary condition is imposed on the rotor surface as shown in Figure 6.

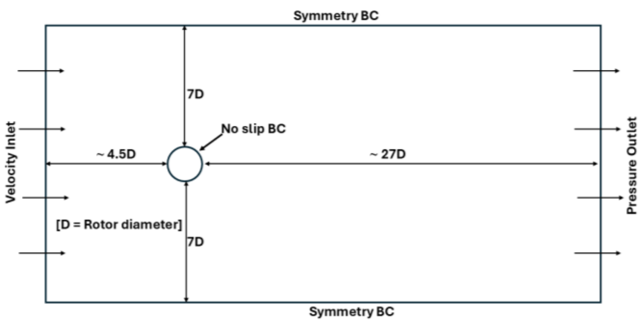

Figure 6: Computational domain for 2D rotor simulations (not in scale)

The velocity inlet and pressure outlet are used to prescribe inflow and outflow conditions, respectively. Figure 7 shows the generated mesh used for the rotor simulations and the mesh is generated using automated meshing option of STAR CCM+. The generated mesh is a polyhedral core mesh with ten-layer prism cells and progressively finer resolution toward the rotor surface. Enhanced mesh refinement is evident around the rotor to accurately capture flow gradients, though no additional refinement in wake region was applied. The first layer is designed to maintain $y^+ < 1$, to properly resolve the near-wall boundary layer and the mesh contain approximately 400,000 cells.

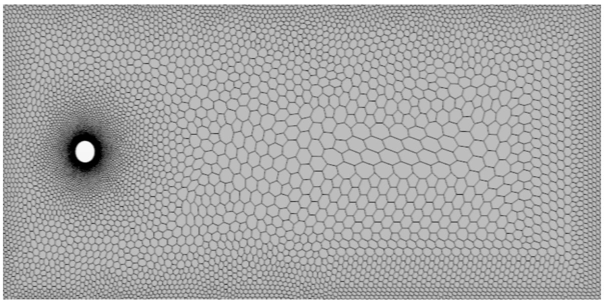

(a)

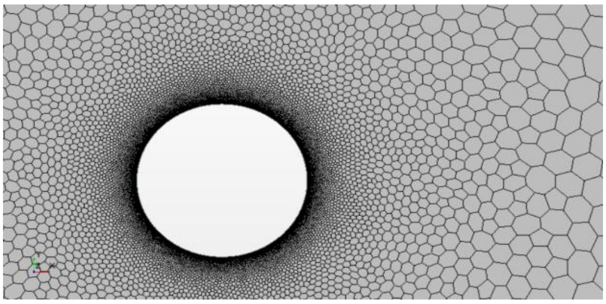

(b)

Figure 7: Generated mesh view: full domain (top) and close-up view around the rotor(bottom)

The 3-D simulation of a single rotor was also performed for the same operating conditions of wind speed and angles as a part of preliminary assessment. The rectangular cube domain has the same dimension as used in 2-D simulations (Figure 6) and the 3-D domain extends approximately ~ 3×H (rotor height) in vertical direction placing the rotor at the bottom of the domain. For the 3-D rotor simulations, the mesh was generated with approximately 1.2 million polyhedral cells in the core region. Local refinement was applied around the rotor, with a minimum cell size of approximately 0.05×D to accurately resolve the flow phenomenon. The boundary-layer mesh with ten prism layers was used, with the first layer positioned to maintain $y^+ < 1$, and a growth ratio of 1.2. Figure 8 shows the generated mesh view of domain and rotor. Figure 9 shows the variation of the lift coefficient (C_L) and drag coefficient (C_D) of three different meshes presenting the mesh-independence study conducted for the 3D rotor simulations. The mesh-independence study was conducted using coarse (0.8 M), baseline (1.2 M), and fine (1.8 M) meshes. As the number of cells increases, C_L exhibits a noticeable decrease, indicating sensitivity to mesh refinement in capturing unsteady flow features around the rotor. C_D shows relatively minor variation, suggesting lower sensitivity to grid resolution. The study uses 1.2 million cells as baseline mesh for the reported result in the paper.

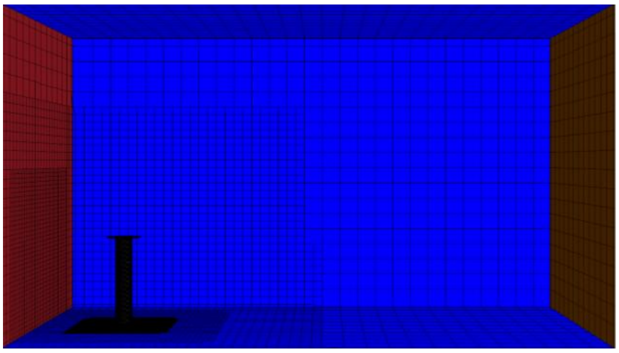

Figure 8: Generated mesh view for 3D rotor case

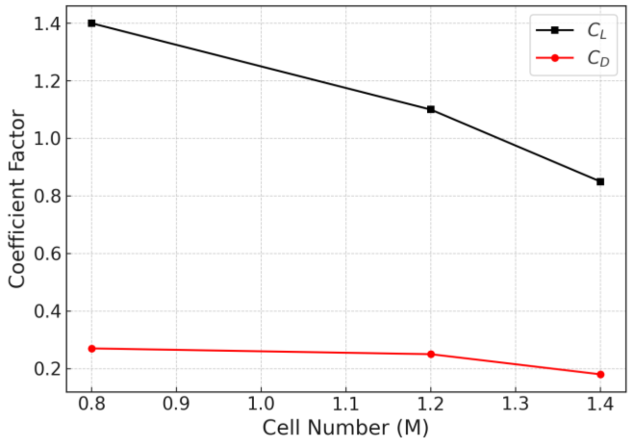

Figure 9: Mesh convergence study

6.1.2 Result Analysis

Figure 10 shows the power consumption by the rotor as computed using the Eq. (9) at different spin ratio and apparent wind. Required power to rotate the rotor increase with increment of spin ratio and wind velocity. Next, we evaluate the potential power savings from the rotor based on the forces computed in numerical simulation for 2-D and 3-D rotor. To find the potential power savings, we consider the reference bare hull resistance at the towing condition. The bare hull resistance at model scale for the JBC as reported by experimental study is 4.289×10^{-3} (Hirata et al., 2020), and total effective power is 43.08 kW at corresponding model speed 1.179 m/s. According to Hussain et al. (2022), the overall propulsive efficiency of a conventional rudder–propeller system on a cargo ship ranges from approximately 0.60 to 0.65. In this study, an efficiency of 0.63 is assumed, resulting in a brake power requirement of 68 kW. Figures 11 and 12 present the potential power savings achieved using four Flettner rotors at various angles of attack and spin ratios at two inflow wind speeds (1.26 m/s and 1.90 m/s).

The estimated savings are calculated by extracting lift and drag forces from CFD simulations and applying Equation (4) to determine the forward thrust generated by the rotors. This thrust is subtracted from the total resistance to computing the new power requirement. It is important to note that the power consumed by the rotors is also accounted for by adding it to the baseline power requirement without rotors. Additionally, the effect of increased wind speed on ship resistance is not considered in the baseline model for the model speed.

The 2D results show a clear increase in power reduction with higher spin ratios, particularly for lower angles of attack (e.g., 120°–135°), with peak savings exceeding 15–30%. In the 3D simulations, the trends remain consistent but show slightly reduced effectiveness due to three-dimensional effects and boundary layer development. Figures 13 and 14 show the velocity and dynamic pressure contours around the rotor at spin ratios 3 and 4, for both 2D and 3D simulations. It is noted both contours are scaled to corresponding full scale velocity. As the spin ratio increases, both the induced velocity and pressure differential around the rotor intensify, indicating stronger lift generation. Compared to the 2D case, the 3D simulations exhibit more diffused wake regions and reduced pressure gradients due to three-dimensional effects and flow development in the spanwise direction.

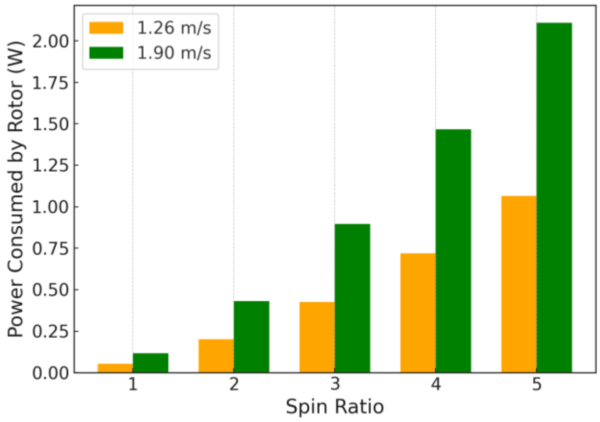

Figure 10: Flettner Rotor Power Consumption for 2D and 3D Rotor

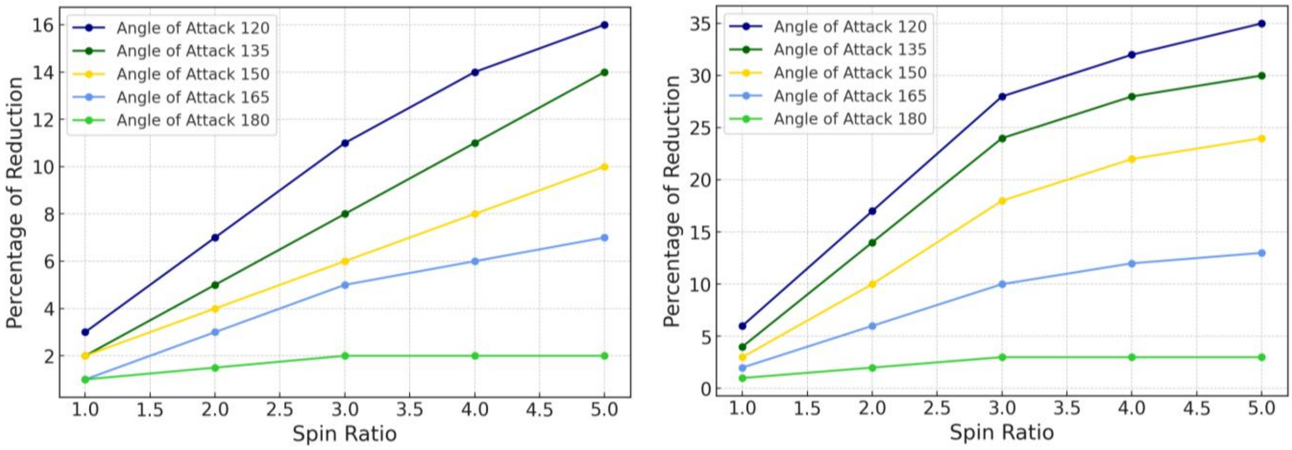

Figure 11: Potential reduction in ship power requirement obainted by 2D rotor analysis: wind speed 1.26 m/s (top) and 1.90 m/s (bottom)

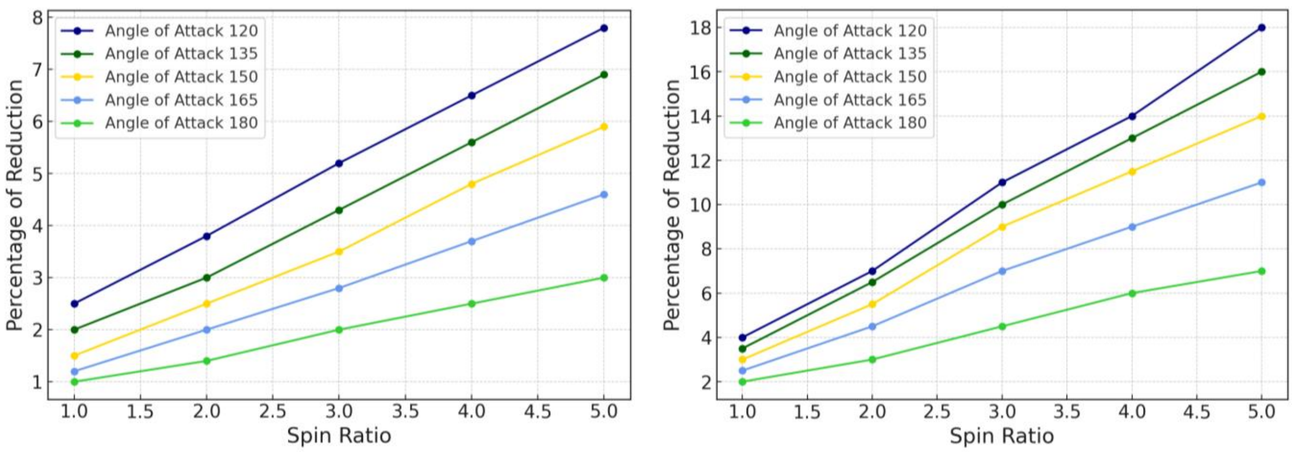

Figure 12: Potential reduction in ship power requirement obainted by 3D rotor analysis: wind speed 1.26 m/s (top) and 1.90 m/s (bottom)

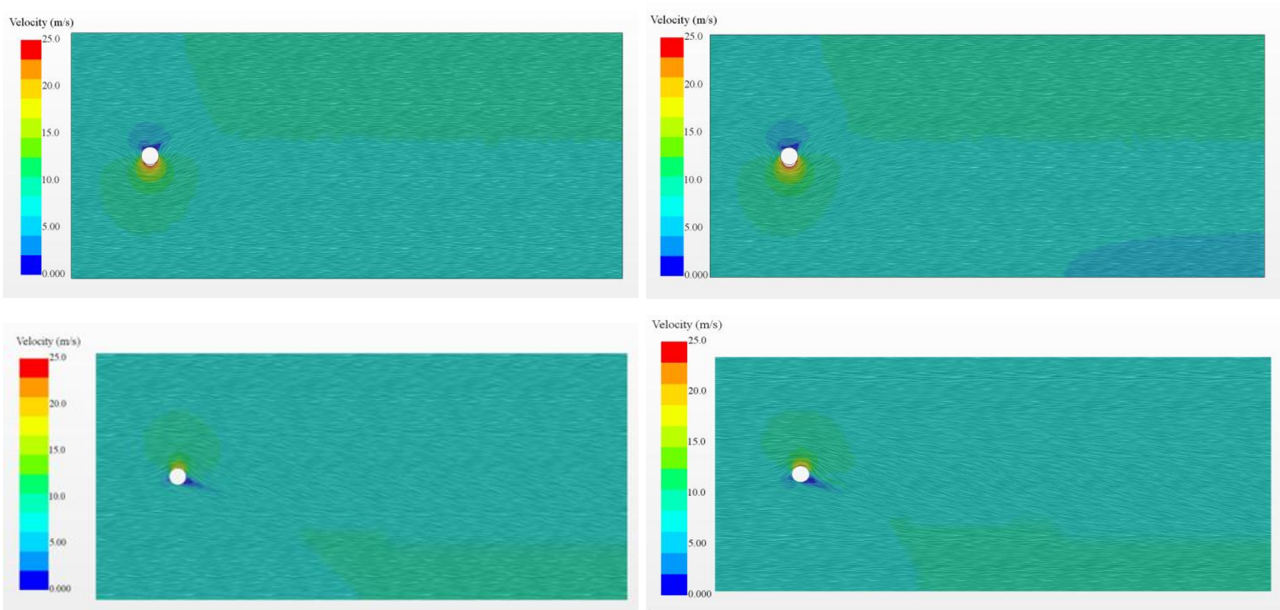

Figure 13: Velcoity contour at spin ratio 3 (left column) and 4 (right column) and appanrant wind speed 1.26 m/s : 2D case (top row) and 3D case(bottom row)

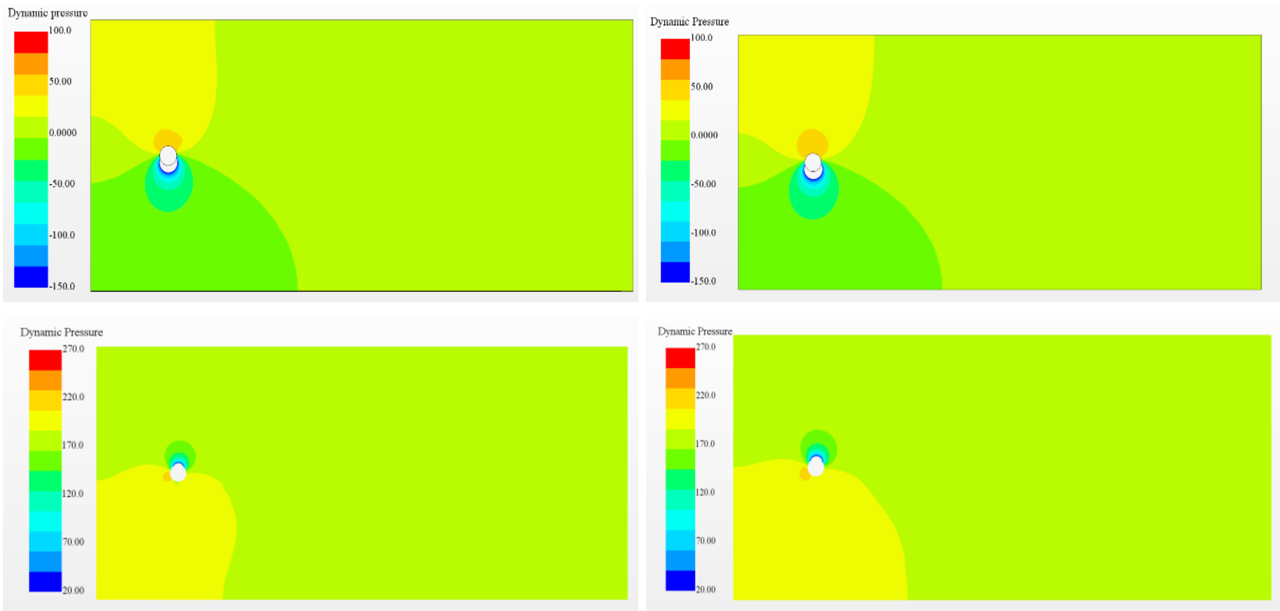

Figure 14: Dynamic pressure contour at spin ratio 3 (left column) and 4 (right column) and appanrant wind speed 1.26 m/s: 2D case (top row) and 3D case(bottom row)

Based on these results, the optimal configuration corresponds to a spin ratio of 4–5 and angle of attack between 120° and 135°, yielding up to 18% net power savings at full scale under wind speeds of approximately 8–12 m/s. Thus, the main takeaway from this preliminary assessment shows the potentiality of the rotors to reduce power requirements and ultimately the fuel savings. As in this preliminary assessment, we didn't consider rotor-rotor interaction and rotor, ship interaction, which are also very important to assess the actual operational performance. Thus, in the next section, we will assess the performance of the rotor installed on the ship model.

6.2 Analysis of Rotor-To-Rotor Interaction

6.2.1 Computational Setup and Mesh Description

The multiphase VOF simulation is conducted for the ship with rotors under towing conditions to primarily evaluate rotor-to-rotor interactions and the influence of the rotors on total ship resistance. In this setup, the rotors are modeled as static structures mounted on the deck, with a wind speed of 1.90 m/s and a 180-degree angle of attack for both configuration of the rotor as shown in Figure 5. The Froude number of the model is 0.142, corresponding to a towing speed of 1.179 m/s. While this simplified approach is not sufficient to fully capture the complex interactions among multiple rotors, it nonetheless provides useful insights, particularly regarding how the flow interacts with the rotors and how much additional resistance they contribute to the overall ship resistance.

The same numerical methodologies used for the single isolated rotor are applied here as well. Figure 15 shows the computational domain used for full rotor-ship configuration simulations. The domain extends approximately 1.5 Lpp upstream, 2.5 Lpp downstream, 1.5 Lpp vertically bottom and 1.0 Lpp from deck to top boundary. The width of the domain was 1.5 Lpp and symmetrical condition was applied along the center line of the ship spanwise to reduce computational time.

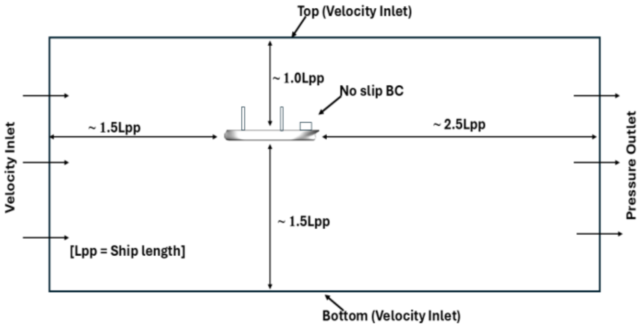

Figure 15: Side view of the computational domain for ship simulation (not in scale)

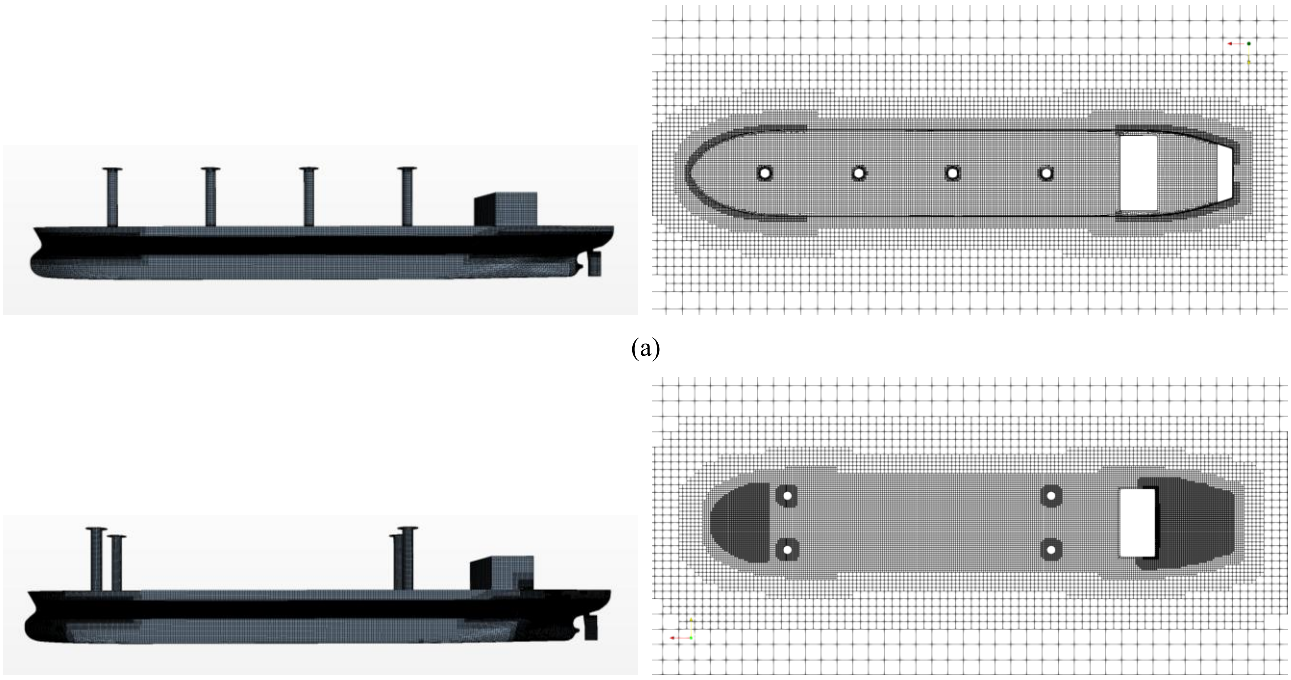

(a)

(b)

Figure 16: Genereted mesh view on ship and rotors for two different configurations: (a) in-line arrangement full view and a cross sectional view (top) and (b) 2 × 2 staggered arrangement full view and a cross sectional view (bottom)

Figure 16 shows the mesh on the ship hull surface and rotor for two different rotor arrangement configurations. A refinement was applied at the free surface region of the ship hull to capture wave resistance properly. Some localized refinement at the bow and aft side at the rudder region were also applied. Mesh coarsening was applied at the inlet/outlet & far-field as these are less important flow feature areas. A total of 4.0 M cells were used in this study.

6.2.1 Results Analysis

The computed total resistance coefficients for the in-line arrangement are 4.72×10^{-3} and the 2×2 staggered arrangement is 4.78×10^{-3}. The reported experimental data for the same operating conditions but with bare hull only no deck or rotor on the deck is 4.289×10^{-3} (Hirata et al., 2020). Based on the experimental data, the total resistance of the model at Fr = 0.149 is 36 N, whereas the two rotor cases give about 39.9 N and 40.5 N, respectively, for the same model speed.

The model with rotor indeed increases the total resiatnces almost about 10-11% comapred to experimnetal data. While major portion of these deviation comes due to the repsence of rotor on the deck and accomodation deck, it also comprise the numerical uncertainity as well. We are not evaluating numerical uncertainty in this study as we are soley focusing on just to get a preliminary undertanding how the rotors and their arrangement affecting in a broader picture as well how flow aerodoynmics behave among the rotors. The total resiatnce predicted for both cases are almost same indicating the rotor arrangement which has minimal influence on the resisatnce. However, as the rotors were kept fixed, it is not possible to calculate the amount of lift force gerenated by a rotating rotors from these set of simulations.

Figure 17 shows the visulation of the flow of this simualtions. As it is seen in the figure, the flow is no longer uniform over the deck due to the presence of rotors. We suspect that the downstream rotors operate in the wake of the upstream ones for the four in line rotor arrangement.

This causes reduced apparent wind speed and turbulent flow structures, leading to weaker lift generation for the aft rotors. On the other hand, in 2×2 staggert arragement, the rotors are laterally offset, minimizing direct wake interference. Each rotor has better access to relatively undisturbed flow, improving aerodynamic efficiency. Thus more favorable flow interaction should allow for higher net thrust and balanced performance across rotors.

(a) (b)

Figure 17: Flow passed around the rotors: in-line arrangement in (a) and 2 × 2 staggered arrangement in (b)

7. CONCLUSIONS

To summarize, the numerical study assessing the preliminary performance of a rotor-assisted ship was carried out by solving the unsteady Reynolds-Averaged Navier–Stokes (RANS) equations using the SST k–ω turbulence model. A systematic approach was adopted, beginning with 2D and 3D simulations of isolated rotors, followed by an investigation of rotor-to-rotor interactions with rotors installed on the main deck of the model ship.

The key outcome of the study highlights the potential of Flettner rotors to reduce power requirements and achieve fuel savings. Although determining the optimal configuration and operating conditions remains a challenge, results indicate that a spin ratio of 4–5 and an angle of attack between 120° and 135° could lead to up to 18% net power savings at full scale under wind speeds of approximately 8–12 m/s. Towing simulations further revealed that rotors installed on the deck can increase the ship's total resistance, and that a 2 × 2 staggered arrangement offers superior aerodynamic performance compared to an in-line configuration of four rotors.

That said, the study has certain limitations. Notably, the results have not been validated against experimental data, and a rigorous verification study is needed to accurately quantify the additional resistance introduced by the rotors. While an attempt to assess the rotor-to-rotor interaction is performed, interaction between rotors to ship remain unevaluated which might have significant effects on the ship stability and seakeeping performance. Furthermore, as the current simulations were conducted at model scale, a full-scale evaluation is essential to determine the actual fuel savings achievable under real-sea operating conditions.

ACKNOWLEDGMENTS

Authors would like to express their gratitude to the Department of Naval Architecture and Marine Engineering, Military Institute of Science and Technology (MIST), Dhaka-1216, Bangladesh. They also would like to thank the editorial members of MIJST for insightful suggestion.

AUTHOR DECLERATION

The authors declare that they have no known competing financial interests or personal relationships that could have appeared to influence the work reported in this paper.

FUNDING INFORMATION

The project did not receive any funding.

REFERENCES

Bordogna, G., Markey, D. J., Huijsmans, R. H. M., Keuning, J. A., & Fossati, F. V. (2014). Wind-assisted ship propulsion: a review and development of a performance prediction program for commercial ships. In Proceedings of the 11th International Conference on Hydrodynamics, ICHD.

Bordogna, G., Muggiasca, S., Giappinob, S., Bellolib, M., Keuninga, J. A., Huijsmans, R. H. M., & van 't Veer, A. P. (2019). Experiments on a flettner rotor at critical and supercritical reynolds numbers. Journal of Wind Engineering and Industrial Aerodynamics, 188(1), 19–29. https://doi.org/10.1016/j.jweia.2019.02.006

Chen, W., Wang, H., & Liu, X. (2023). Experimental investigation of the aerodynamic performance of Flettner rotors for marine applications. Ocean Engineering, 281, 115006. https://doi.org/10.1016/j.oceaneng.2023.115006

Copuroglu, H. I., & Pesman, E. (2018). Analysis of flettner rotor ships in beam waves. Ocean Engineering, 150, 352–362. https://doi.org/10.1016/j.oceaneng.2018.01.004

De Marco, A., Mancini, S., Pensa, C., Calise, G., & De Luca, F. (2016). Flettner rotor concept for marine applications: A systematic study. International Journal of Rotating Machinery, 2016(1), 1–12. https://doi.org/10.1155/2016/3458750

Hirata, N., Kobayashi, H., Hino, T., Toda, Y., Abdel-Maksoud, M., & Stern, F. (2020). Experimental data for JBC resistance, sinkage, trim, self-propulsion factors, longitudinal wave cut and detailed flow with and without an energy saving circular duct. Numerical

Ship Hydrodynamics, 23–51. https://doi.org/10.1007/978-3-030-47572-7_2

Hussain, M. D., & Amin, O. M. (2021). A comprehensive analysis of the stability and powering performances of a hard sail–assisted bulk carrier. Journal of Marine Science and Application, 20(3), 426–445. https://doi.org/10.1007/s11804-021-00219-w

Hussain, M. D., Karim, M. M., & Sasaki, N. (2022). Numerical assessment of the scale effects on the propulsive performance of a ship with gate rudder system. Ocean Engineering, 249, 110889. https://doi.org/10.1016/j.oceaneng.2022.110889

Hussain, M. D., Shahnewaz, M., Kabir, S., & Amin, O. M. (2018). Numerical investigation of the stability and power prediction of a sail-based wind propulsion system for a cargo ship. AIP Conference Proceedings, 1980(1). https://doi.org/10.1063/1.5044374

Joung, T.-H., Kang, S.-G., Lee, J.-K., & Ahn, J. (2020). The IMO initial strategy for reducing greenhouse gas(ghg) emissions, and its follow-up actions towards 2050. Journal of International Maritime Safety, Environmental Affairs, and Shipping, 4(1), 1–7. https://doi.org/10.1080/25725084.2019.1707938

Kolodziejski, M., & Sosnowski, M. (2025). Review of wind-assisted propulsion systems in maritime transport. Energies, 18(4), 897. https://doi.org/10.3390/en18040897

Kume, K., Hamada, T., Kobayashi, H., & Yamanaka, S. (2022). Evaluation of aerodynamic characteristics of a ship with Flettner rotors by wind tunnel tests and rans-based CFD. Ocean Engineering, 254, 111345. https://doi.org/10.1016/j.oceaneng.2022.111345

Lele, A., & Rao, K. V. S. (2017, April). Net power generated by Flettner rotor for different values of wind speed and ship speed. In 2017 International Conference on Circuit, Power and Computing Technologies (ICCPCT) (pp. 1-6). IEEE.

Li, B., Zhang, R., Zhang, B., Yang, Q., & Guo, C. (2021). An assisted propulsion device of vessel utilizing wind energy based on magnus effect. Applied Ocean Research, 114, 102788. https://doi.org/10.1016/j.apor.2021.102788

Li, J., Lin, H., Sun, C., Jiao, B., Sun, G., & Cao, F. (2024). Analysis of aerodynamic performance and application of Flettner rotor. Journal of the Institution of Engineers (India) Series C. https://doi.org/10.1007/s40032-024-01073-9

Lu, R., & Ringsberg, J. W. (2019). Ship energy performance study of three wind-assisted ship propulsion technologies including a parametric study of the flettner rotor technology. Ships and Offshore Structures, 15(3), 249–258. https://doi.org/10.1080/17445302.2019.1612544

Menter, F. R. (1994). Two-equation eddy-viscosity turbulence models for engineering applications. AIAA Journal, 32(8), 1598–1605. https://doi.org/10.2514/3.12149

Seddiek, I. S., & Ammar, N. R. (2021). Harnessing wind energy on merchant ships: Case study flettner rotors onboard bulk carriers. Environmental Science and Pollution Research, 28(25), 32695–32707. https://doi.org/10.1007/s11356-021-12791-3

Tillig, F., & Ringsberg, J. W. (2020). Design, operation and analysis of wind-assisted cargo ships. Ocean Engineering, 211, 107603. https://doi.org/10.1016/j.oceaneng.2020.107603

Traut, M., Gilbert, P., Walsh, C., Bows, A., Filippone, A., Stansby, P., & Wood, R. (2014). Propulsive power contribution of a kite and a flettner rotor on selected shipping routes. Applied Energy, 113, 362–372. https://doi.org/10.1016/j.apenergy.2013.07.026

Wang, K., Li, Z., Zhang, R., Ma, R., Huang, L., Wang, Z., & Jiang, X. (2024). Computational fluid dynamics-based ship energy-saving technologies: A comprehensive review. Renewable and Sustainable Energy Reviews, 207, 114896. https://doi.org/10.1016/j.rser.2024.114896